A Comparison of Three Magnetics Integration Solutions for the Two-Inductor Boost Converter

Quan Li
Faculty of Engineering and Physical Systems
Central Queensland University
Rockhampton, Queensland, Australia
q.li@cqu.edu.au

Peter Wolfs
Faculty of Engineering and Physical Systems
Central Queensland University
Rockhampton, Queensland, Australia
p.wolfs@cqu.edu.au

ABSTRACT

The two-inductor boost converter presents significant advantages over other boost topologies but requires three separate magnetic devices. This paper introduces a systematic approach in developing the magnetic integration schemes for the hard-switched two-inductor boost converter. Both the magnetic core integration and the winding integration methods are used. Design equations are explicitly established for the equivalent input and transformer magnetizing inductance values. The theoretical waveforms are provided for all three magnetic integration solutions. Experimental waveforms are also provided for the two solutions that are suited to the hard-switched implementations.

1. INTRODUCTION

The two-inductor boost converter is a favourable topology for transforming the low-voltage high-current dc input to a high-voltage dc output [1] and possesses several advantages such as high dc voltage gain, low switch voltage stress, easy transformer volt-second balance and a relaxed diode reverse recovery requirement [2], [3]. The hard-switched converter with a voltage doubler rectifier is shown in Figure 1. In the effort to reduce the converter size, soft-switching technique has been employed in the converter [4]. However, the two-inductor boost converter does require at least three separate magnetic components including two inductors and one transformer, which contribute to the size and the cost [5]. Magnetic core integration theory was formally presented more than twenty years ago as a way to assist in reducing the size of the switch mode power converters [6]-[8]. One application can be traced back to early 1930's [9]. Recently, winding integration has been proposed to reduce winding cost and to improve efficiency [10]. These integrated magnetic approaches have been widely applied to the current-doubler rectifier circuits [11]-[16].

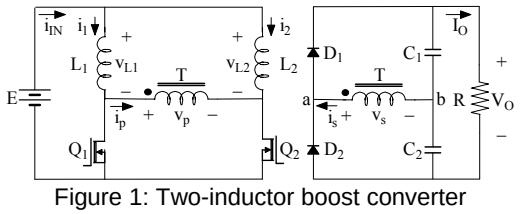

Figure 1: Two-inductor boost converter

This paper systematically develops three magnetic integration solutions for the two-inductor boost converter. Among these, Structure A was independently proposed by the authors in [17] and by Gao and Ayyannar in [18], Structure B was proposed by the authors in [19] and Structure C was proposed in [20]. This paper presents a detailed analysis of the equivalent inductances, the peak flux densities and the current ripples for the new magnetic structures. Both of the theoretical and the experimental waveforms are provided in the paper.

2. STATE ANALYSIS

The state analysis is conducted in the two-inductor boost converter with discrete magnetics, as shown in Table 1. D is the duty ratio of the MOSFETs and must be greater than 50% to prevent an open circuit of the currents in the two inductors. T_s is the switching period. $L_1 = L_2 = L$ is the input inductance. L_{ms} is the transformer magnetizing inductance reflected to the secondary side. N_p and N_s are respectively the primary and the secondary number of turns of the transformer T. The equations in Table 1 will be used to obtain the equivalent inductance values of the converter with the integrated magnetics. The current waveforms are shown in Figure 2.

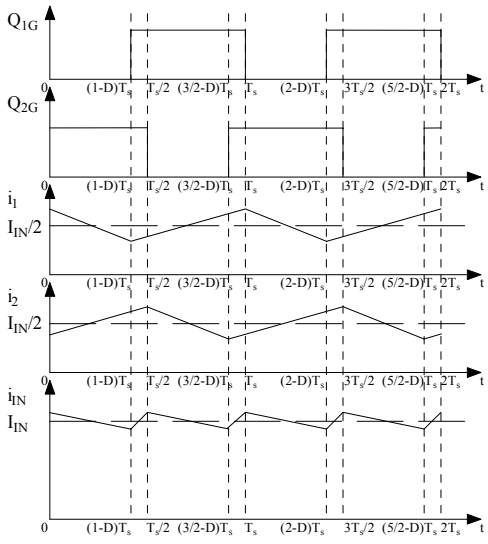

Figure 2: Current waveforms

3. MAGNETIC CORE INTEGRATION

3.1. CIRCUIT DIAGRAM

A first magnetic integration solution is to combine the three cores to a single core while maintaining the four windings required by the two inductors and the transformer.

State	Circuit Diagram	Circuit Equations
State (1) $0 < t < (1-D)T_s$ Q_1 off, Q_2 on	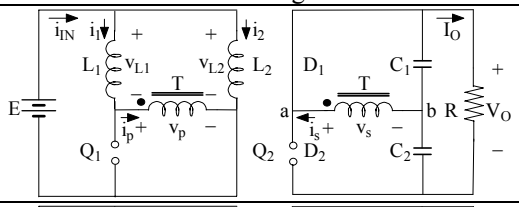	$\frac{d(i_1+i_2)}{dt} = \frac{1}{L}(2E - \frac{N_p}{N_s}v_s)$ (1) $\frac{di_s}{dt} = \frac{N_p}{N_s}\cdot\frac{E}{L} - \left[\frac{1}{L_{ms}} + \left(\frac{N_p}{N_s}\right)^2\frac{1}{L}\right]v_s$ (2)
State (2) $(1-D)T_s < t < \frac{T_s}{2}$ Q_1 and Q_2 on	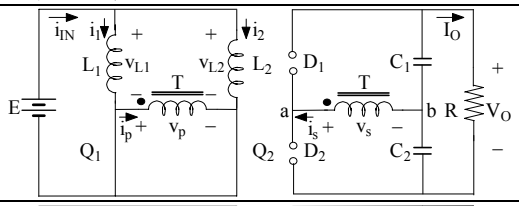	$\frac{d(i_1+i_2)}{dt} = \frac{1}{L}2E$ (3) $\frac{di_s}{dt} = 0$ (4)
State (3) $\frac{T_s}{2} < t < (\frac{3}{2}-D)T_s$ Q_1 on, Q_2 off	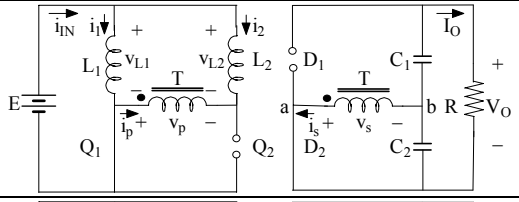	$\frac{d(i_1+i_2)}{dt} = \frac{1}{L}(2E + \frac{N_p}{N_s}v_s)$ (5) $\frac{di_s}{dt} = -\frac{N_p}{N_s}\cdot\frac{E}{L} - \left[\frac{1}{L_{ms}} + \left(\frac{N_p}{N_s}\right)^2\frac{1}{L}\right]v_s$ (6)
State (4) $(\frac{3}{2}-D)T_s < t < T_s$ Q_1 and Q_2 on	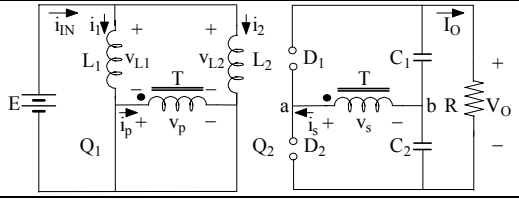	$\frac{d(i_1+i_2)}{dt} = \frac{1}{L}2E$ $\frac{di_s}{dt} = 0$

Table 1: State analysis of the two-inductor boost converter with discrete magnetics

This approach is named as Structure A and the converter circuit diagram with Structure A magnetic integration is shown in Figure 3. The voltages across the three windings in the converter primary side must satisfy:

$$v_p = v_{L2} - v_{L1} \tag{7}$$

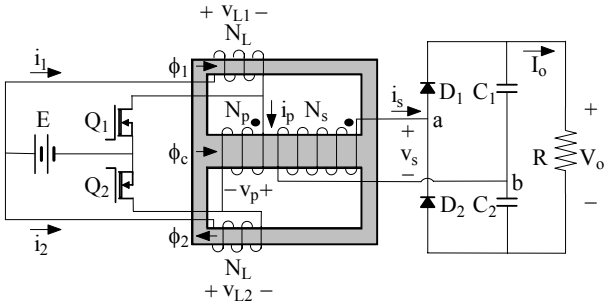

Figure 3: Structure A magnetic integration

Application of Faraday's Law yields:

$$N_p \frac{d\phi_c}{dt} = N_L \frac{d\phi_2}{dt} - N_L \frac{d\phi_1}{dt} \tag{8}$$

where N_L is the number of the turns of the inductors L_1 and L_2 and ϕ_1, ϕ_2 and ϕ_c are respectively the instantaneous fluxes in the outer and the centre core legs. The flux in the centre core leg is:

$$\phi_c = \phi_2 - \phi_1 \tag{9}$$

Manipulations of Equations (8) and (9) yield:

$$N_p = N_L \tag{10}$$

Equation (10) is the inherent constraint for Structure A.

3.2. EQUIVALENT INDUCTANCES

In order to obtain the equivalent input and magnetizing inductances of the converter with Structure A magnetic integration, the converter must be analysed under three different operating conditions.

- State (1) ($v_s > 0$): In this state, Q_1 is off while Q_2 is on and i_1 flows in the transformer primary winding. The magnetic circuit is drawn in Figure 4(a), where $\Re_c$ and $\Re_o$ are respectively the reluctances of the centre and the outer core legs. The fluxes in the two outer core legs are:

$$\phi_1 = \frac{N_p(i_1+i_2)}{\Re_o + 2\Re_c}\cdot\frac{\Re_c}{\Re_o} + \frac{N_s i_s}{\Re_o + 2\Re_c} \tag{11}$$

$$\phi_2 = \frac{N_p(i_1+i_2)}{\Re_o + 2\Re_c}\left(1 + \frac{\Re_c}{\Re_o}\right) - \frac{N_s i_s}{\Re_o + 2\Re_c} \tag{12}$$

Faraday's Law gives:

$$N_p \frac{d\phi_1}{dt} = E - \frac{N_p}{N_s}v_s \tag{13}$$

$$N_p \frac{d\phi_2}{dt} = E \tag{14}$$

Substitution of Equations (11) and (12) into Equations (13) and (14) yields:

$$\frac{d(i_1+i_2)}{dt} = \frac{\Re_o}{N_p^2}\left(2E - \frac{N_p}{N_s}v_s\right) \tag{15}$$

$$\frac{di_s}{dt} = \frac{\Re_o}{N_p N_s}E - \frac{\Re_o + \Re_c}{N_s^2}v_s \tag{16}$$

By defining L_a and L_b to be

$$L_a = N_p^2 / \Re_o \tag{17}$$

$$L_b = 2N_s^2 / (\Re_o + 2\Re_c) \tag{18}$$

Equations (15) and (16) can be rewritten as:

$$\frac{d(i_1 + i_2)}{dt} = \frac{1}{L_a}\left(2E - \frac{N_p}{N_s} v_s\right) \tag{19}$$

$$\frac{di_s}{dt} = \frac{N_p}{N_s} \cdot \frac{E}{L_a} - \left[\frac{1}{L_b} + \left(\frac{N_p}{N_s}\right)^2 \frac{1}{2L_a}\right] v_s \tag{20}$$

- State (3) ($v_s < 0$): In this state, Q_1 is on while Q_2 is off and i_2 flows in the transformer primary winding. The magnetic circuit is drawn in Figure 4(b) and the following equations can be obtained.

$$\frac{d(i_1 + i_2)}{dt} = \frac{1}{L_a}\left(2E + \frac{N_p}{N_s} v_s\right) \tag{21}$$

$$\frac{di_s}{dt} = -\frac{N_p}{N_s} \cdot \frac{E}{L_a} - \left[\frac{1}{L_b} + \left(\frac{N_p}{N_s}\right)^2 \frac{1}{2L_a}\right] v_s \tag{22}$$

- States (2) and (4) ($v_s = 0$): In these two states, Q_1 and Q_2 are both on and the transformer primary current is zero. The magnetic circuit is drawn in Figure 4(c) and the following equation can be obtained. Equation (4) is also valid in these states.

$$\frac{d(i_1 + i_2)}{dt} = \frac{1}{L_a} 2E \tag{23}$$

Comparisons of Equations (19) to (23) with their discrete magnetic counterparts in Table 1 yield:

$$L = N_p^2 / \Re_o \tag{24}$$

$$L_{ms} = N_s^2 / \Re_c \tag{25}$$

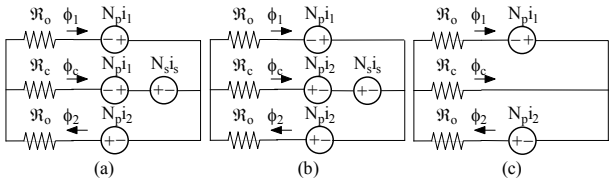

Figure 4: Structure A
(a) State (1) (b) State (3) (c) States (2) and (4)

3.3. DC GAIN

Due to the flux continuity, the output voltage is:

$$V_O = \frac{N_s}{N_p} \cdot \frac{2}{1-D} E \tag{26}$$

3.4. PEAK FLUX DENSITIES

The dc and ac fluxes are analysed separately. According to Figure 4(a), the instantaneous fluxes in Structure A in State (1) are restricted by:

$$\Re_o \phi_1 + \Re_o \phi_2 = N_p (i_1 + i_2) = N_p i_{IN} \tag{27}$$

$$\Re_o \phi_1 - \Re_c \phi_c = N_s i_s \tag{28}$$

If Φ_1, Φ_2, Φ_c, I_{IN} and I_s are the dc components of ϕ_1, ϕ_2, ϕ_c, i_{in} and i_s in State (1), $N_s I_s = N_p I_{IN} / 2$ can be obtained through the power balance of the converter. Equations (9), (27) and (28) can be rewritten to the following equations, which are now valid over the entire switching period as Φ_1, Φ_2, Φ_c and I_{IN} are also the dc variables in one complete switching period.

$$\Phi_c = \Phi_2 - \Phi_1 \tag{29}$$

$$\Re_o \Phi_1 + \Re_o \Phi_2 = N_p I_{IN} \tag{30}$$

$$\Re_o \Phi_1 - \Re_c \Phi_c = N_p I_{IN} / 2 \tag{31}$$

Solving for Φ_1, Φ_2 and Φ_c yields:

$$\Phi_1 = \Phi_2 = N_p I_{IN} / (2\Re_o) \tag{32}$$

$$\Phi_c = 0 \tag{33}$$

The ac fluxes in the individual core legs are:

$$|\Delta\phi_1| = |\Delta\phi_2| = EDT_s / N_p \tag{34}$$

$$|\Delta\phi_c| = ET_s / N_p \tag{35}$$

Therefore from Equations (32) to (35), the peak flux density in each core leg can be calculated as:

$$B_{1,\max} = B_{2,\max} = \frac{N_p I_{IN}}{\Re_o A_c} + \frac{EDT_s}{N_p A_c} \tag{36}$$

$$B_{c,\max} = \frac{ET_s}{2N_p A_c} \tag{37}$$

where A_c is the cross section area of the centre core leg. The cross section area of the outer core leg is normally made to be half that of the centre core leg.

The flux waveforms are shown in Figure 5. It can be seen that the dc fluxes in the two outer core legs cancel and the ac fluxes add together in the centre core leg.

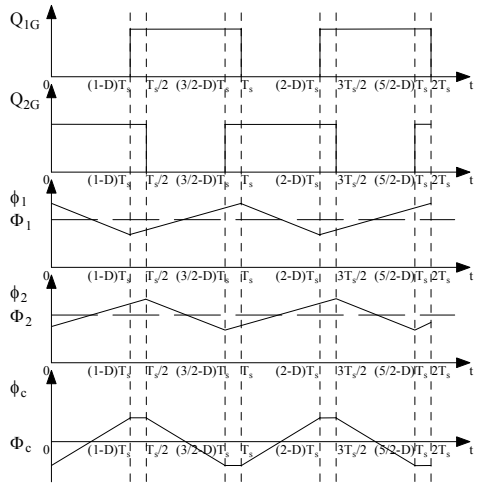

Figure 5: Flux waveforms in Structure A core

3.5. CURRENT RIPPLES

Equations (27) and (28) can be rewritten as:

$$\Delta i_{IN} = (\Re_o \Delta\phi_1 + \Re_o \Delta\phi_2)/N_p \quad (38)$$

$$\Delta i_s = (\Re_o \Delta\phi_1 - \Re_c \Delta\phi_c)/N_s \quad (39)$$

The ac components in i_{IN}, i_1, i_2 and i_s can be respectively solved to be:

$$|\Delta i_{IN}| = \frac{(2D-1)\Re_o E T_s}{N_p^2} \quad (40)$$

$$|\Delta i_1| = |\Delta i_2| = \frac{D\Re_o E T_s}{N_p^2} \quad (41)$$

$$|\Delta i_s| = \frac{N_p}{N_s} \cdot \frac{(D\Re_o + \Re_c) E T_s}{N_p^2} \quad (42)$$

4. WINDING INTEGRATIONS

The transformer primary winding can be merged with the inductor windings. The combined windings must be located on the outer core legs to achieve symmetrical operation. Topographically, there are four ways to place the two combined windings onto the outer core legs resulting in different combinations of the directions of the two fluxes in the outer core legs. The number of the winding structures can be finally reduced to two, as shown in Figure 6. In Figure 6(a), the flux changes generated by the two individual windings are of the same direction in the two outer core legs and of different directions in the centre core leg. In Figure 6(b), it is vice versa. As the transformer secondary flux must be alternating, the secondary winding in Fig. 6(a) must be placed on the centre core leg and in Figure 6(b) on the two outer core legs. The approach which uses a single secondary winding on the centre core leg is named as Structure B, as shown in Figure 7. The approach which uses two secondary windings on the outer core legs is named as Structure C, as shown in Figure 8 [20].

The equivalent input and magnetizing inductances, the peak flux densities in the individual core legs and the current ripples of all three integrated magnetic structures are listed in Table 2. In Structure B the dc fluxes in the two outer core legs cancel in the centre core leg while the ac fluxes add together. In Structure C, the dc fluxes in the two outer core legs add together in the centre core leg while the ac fluxes cancel. This leads to a much lower core loss in the centre core leg [21]. The flux and current waveforms of Structures B and C are respectively shown in Figures 9(a) and (b). In Structure C, a variation can be developed by adding another winding in the centre core leg. Figure 10 shows the electrical circuit and the corresponding magnetic circuit for the magnetic core. The winding on the centre core leg acts as an additional input inductance but does not affect the converter dc gain. One centre-leg turn is effective as two outer-leg turns in the contribution to the input inductance. The equivalent input and magnetizing inductances can be respectively obtained as:

$$L = (N_p + 2N_c)^2 / (\Re_o + 2\Re_c) \quad (43)$$

$$L_{ms} = \frac{2N_s^2}{\Re_o - (\Re_o + 2\Re_c) N_p^2 / (N_p + 2N_c)^2} \quad (44)$$

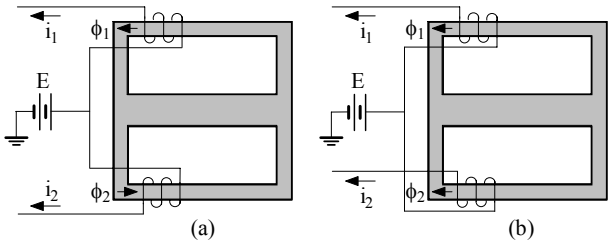

Figure 6: Two ways to wind the two combined windings

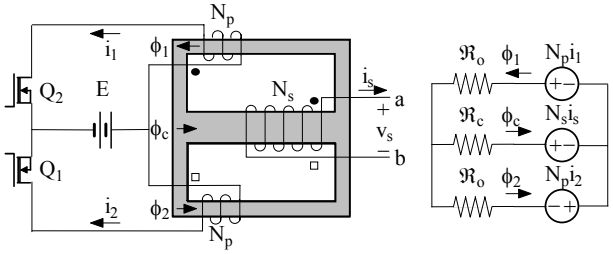

Figure 7: Structure B magnetic integration
(a) Electrical circuit (b) Magnetic circuit

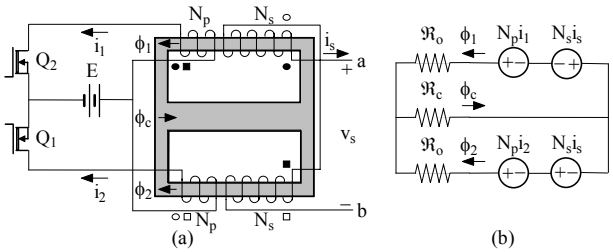

Figure 8: Structure C magnetic integration
(a) Electrical circuit (b) Magnetic circuit

5. EXPERIMENTAL RESULTS

The experimental results of Structure A using an ETD39 core with a 0.5 mm air gap in each of the two outer legs are shown in Figure 11. The top two waveforms are the ac components of fluxes ϕ_1 and ϕ_c obtained through integrating of the voltage of a single search turn wound on the core leg. The bottom two waveforms are the currents i_1 and i_{IN}. They match well with the theoretical waveforms in Figures 2 and 5. The same set of waveforms of Structure C using an ETD39 core with a 0.5 mm air gap in the centre leg only is shown in Figure 12. It can be seen that for the same amount of flux ripple in the outer leg, the flux ripple in the centre leg of this structure is much smaller than that of Structure A. Structure B presents high leakage inductance and therefore is only suited to the resonant converter implementations [19].

6. CONCLUSIONS

This paper provides a generic approach of the magnetic integration of the two inductors and the transformer in the hard-switched two-inductor boost converter. Three magnetic integration solutions are possible and they are thoroughly investigated. The equivalent input and transformer magnetizing inductances of the two-inductor boost converter with the integrated magnetics are established and the comparison of the main features of the three integrated magnetic structures is provided. The experimental results shown at the end of the paper validate the theoretical analysis.

Item	Structure A	Structure B	Structure C
Number of Windings	4	3	4
Input Inductance L	$\frac{N_p^2}{\Re_o}$	$\frac{N_p^2}{\Re_o}$	$\frac{N_p^2}{\Re_o + 2\Re_c}$
Magnetizing Inductance L_{ms}	$\frac{N_s^2}{\Re_c}$	$\frac{N_s^2}{\Re_c}$	$-\frac{N_s^2}{\Re_c}$
DC Gain V_O/E	$\frac{N_s}{N_p}\cdot\frac{2}{1-D}$	$\frac{N_s}{N_p}\cdot\frac{2}{1-D}$	$\frac{N_s}{N_p}\cdot\frac{2}{1-D}$
Peak Flux Density $B_{1,max}$, $B_{2,max}$	$\frac{N_p I_{IN}}{\Re_o A_c}+\frac{EDT_s}{N_p A_c}$	$\frac{N_p I_{IN}}{\Re_o A_c}+\frac{EDT_s}{N_p A_c}$	$\frac{N_p I_{IN}}{(\Re_o + 2\Re_c)A_c}+\frac{EDT_s}{N_p A_c}$
Peak Flux Density $B_{c,max}$	$\frac{ET_s}{2N_p A_c}$	$\frac{ET_s}{2N_p A_c}$	$\frac{N_p I_{IN}}{(\Re_o + 2\Re_c)A_c}+\frac{E(2D-1)T_s}{2N_p A_c}$
Current Ripple Δi_{IN}	$\frac{(2D-1)\Re_o}{N_p^2}ET_s$	$\frac{(2D-1)\Re_o}{N_p^2}ET_s$	$\frac{(2D-1)(\Re_o + 2\Re_c)}{N_p^2}ET_s$
Current Ripple Δi_s	$\frac{N_p}{N_s}\cdot\frac{D\Re_o + \Re_c}{N_p^2}ET_s$	$\frac{N_p}{N_s}\cdot\frac{D\Re_o + \Re_c}{N_p^2}ET_s$	$\frac{N_p}{N_s}\cdot\frac{D\Re_o + (2D-1)\Re_c}{N_p^2}ET_s$
Leakage Inductance	Low	High	Medium
Core Loss	High	High	Low
Minimum Gapped Legs	Two outer core legs	Two outer core legs	The centre core leg

Table 2: Comparisons of three magnetic integration structures

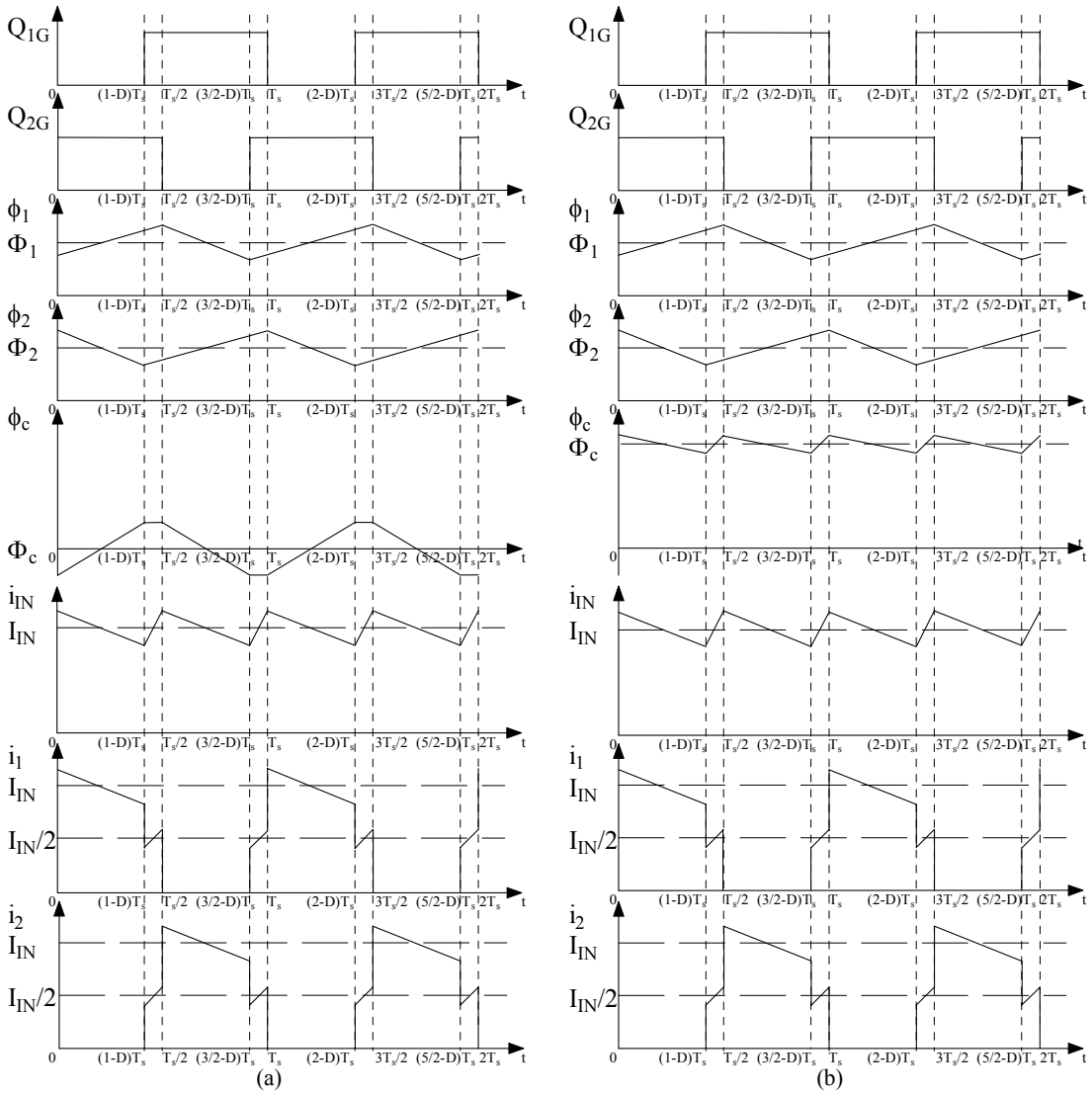

Figure 9: Flux and current waveforms (a) Structure B (b) Structure C

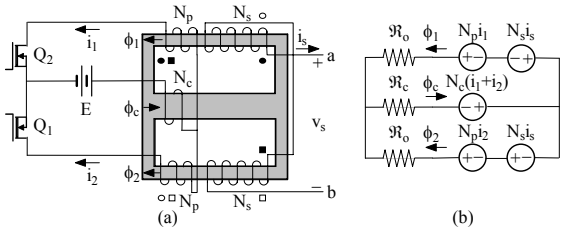

Figure 10: A variation of Structure C magnetic integration (a) Electrical circuit (b) Magnetic circuit

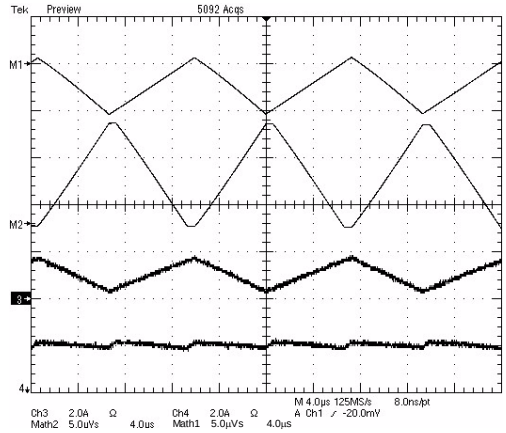

Figure 11: Waveforms for Structure A

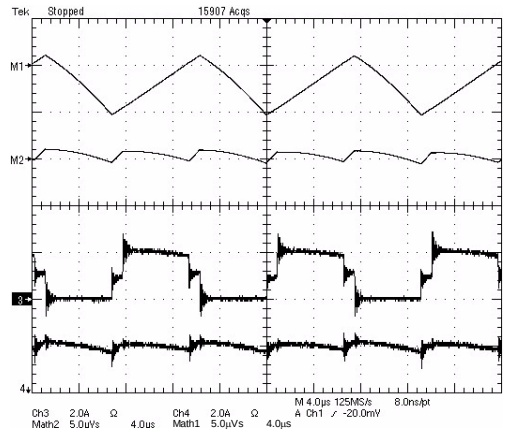

Figure 12: Waveforms for Structure C

REFERENCES

[1] P. J. Wolfs, "A Current-Sourced DC-DC Converter Derived via the Duality Principle from the Half-Bridge Converter," *IEEE Trans. Ind. Electron.*, Vol. 40, No. 1, pp. 139-144, Feb. 1993.

[2] W. C. P. de Aragão Filho and I. Barbi, "A Comparison between Two Current-Fed Push-Pull DC-DC Converters – Analysis, Design and Experimentation," in *Proc. IEEE INTELEC*, 1996, pp. 313-320.

[3] Q. Li, "Development of High Frequency Power Conversion Technologies for Grid Interactive PV Systems," *Master of Engineering Dissertation*, Central Queensland University, Australia, 2002.

[4] P. Wolfs and Q. Li, "An Analysis of a Resonant Half Bridge Dual Converter Operating in Continuous and Discontinuous Modes," in *Proc. IEEE PESC*, 2002, pp.1313-1318.

[5] G. Bloom, "Multi-Chambered Planar Magnetics Blends Inductors and Transformers," *Power Electronics Technology*, Vol. 29, No. 4, pp. 22-34, Apr. 2003.

[6] S. Cuk, "A New Zero-Ripple Switching DC-to-DC Converter and Integrated Magnetics," in *Proc. IEEE PESC*, 1980, pp.12-32; also *IEEE Trans. Magn.*, Vol. 19, No. 2, pp. 57-75, Mar. 1983.

[7] S. Cuk, "New Magnetic Structures for Switching Converters," *IEEE Trans. Magn.*, Vol. 19, No. 2, pp. 75-83, Mar. 1983; also in *Proc. PCI*, 1981.

[8] G. Bloom and R. Severns, "The Generalized Use of Integrated Magnetics and Zero-Ripple Techniques in Switchmode Power Converters," in *Proc. IEEE PESC*, 1984, pp. 15-33.

[9] G. B. Crouse, "Electrical Filter," U.S. Patent 1 920 948, 1 Aug., 1933.

[10] W. Chen, "Low Voltage High Current Power Conversion with Integrated Magnetics," *PhD Dissertation*, Virginia Polytechnic Institute and State University, U.S.A., 1998.

[11] C. Peng, M. Hannigan and O. Seiersen, "A New Efficient High Frequency Rectifier Circuit," in *Proc. HFPC*, 1991, pp. 236-243.

[12] W. Chen, G. Hua, D. Sable and F. Lee, "Design of High Efficiency, Low Profile, Low Voltage Converter with Integrated Magnetics," in *Proc. IEEE APEC*, 1997, pp. 911-917.

[13] P. Xu, Q. Wu, P. Wong and F. C. Lee, "A Novel Integrated Current Doubler Rectifier," in *Proc. IEEE APEC*, 2000, pp. 735-740.

[14] J. Sun and V. Mehrotra, "Unified Analysis of Half-Bridge Converters with Current-Doubler Rectifier," in *Proc. IEEE APEC*, 2001, pp. 514-520.

[15] J. Sun, K. F. Webb and V. Mehrotra, "An Improved Current-Doubler Rectifier with Integrated Magnetics," in *Proc. IEEE APEC*, 2002, pp. 831-837.

[16] J. Sun, K. F. Webb and V. Mehrotra, "Integrated Magnetics for Current-Doubler Rectifiers," *IEEE Trans. Power Electron.*, Vol. 19, No.3, pp. 582-590, May 2004.

[17] Q. Li and P. Wolfs, "A Current Fed Two-Inductor Boost Converter for Grid Interactive Photovoltaic Applications," in *Proc. AUPEC*, 2004.

[18] X. Gao and R. Ayyannar, "A Novel Buck-Cascaded Two-Inductor Boost Converter with Integrated Magnetics," in *Proc. IEEE INTELEC*, 2004, pp. 190-197.

[19] Q. Li and P. Wolfs, "A Leakage-Inductance-Based ZVS Two-Inductor Boost Converter with Integrated Magnetics," *IEEE Power Electron. Lett.*, Vol. 3, No. 2, pp. 67-71, Jun. 2005.

[20] L. Yan and B. Lehman, "Isolated Two-Inductor Boost Converter with One Magnetic Core," in *Proc. IEEE APEC*, 2003, pp. 879-885.

[21] C. P. Steinmetz, "On the Law of Hysteresis," *Proc. IEEE*, Vol. 72, pp. 196-221, Feb. 1984.